International Journal of Advanced Engineering Research and Science (IJAERS)
Peer-Reviewed Journal
ISSN: 2349-6495(P) | 2456-1908(O)
Vol-9, Issue-12; Dec, 2022
Journal Home Page Available: https://ijaers.com/
Article DOI: https://dx.doi.org/10.22161/ijaers.912.35

Crystalline $Bi_{25}FeO_{40}$ Cluster Microspheres as Efficient Photo-Fenton Catalysts for Rhodamine B Degradation

Xuan Sang Nguyen

Environmental Institute, Viet Nam Maritime University, Vietnam

Received: 19 Nov 2022,

Receive in revised form: 10 Dec 2022,

Accepted: 16 Dec 2022,

Available online: 27 Dec 2022

***Keywords*— $Bi_{25}FeO_{40}$; Photo-Fenton; Cluster microspheres.**

***Abstract*—** *In this study, cluster microspheres $Bi_{25}FeO_{40}$ materials were synthesized by a simple method. The characteristic of the obtained products was studied using the X-ray diffraction (XRD), (FESEM) scanning electron microscopy, UV-vis reflectance. Results showed as-prepared products are uniform microspheres with high porosity, which are composed of aggregation nanocrystal speces into an ordered arrangement structure. Their photocatalytic activity in photodegradation of Rhodamine B under visible light was sequentially investigated, indicating the high photocatalytic capacity of as-obtained the cluster $Bi_{25}FeO_{40}$ materials.*

I. INTRODUCTION

Recently, great attention has been paid for the morphology control of nanometer- and micrometer-size catalyst materials because of their interesting physical and chemical properties. Then, these materials can using widely in practice fields[1, 2]. In this respect, a great number of remarkable approaches have been studied to controlling-synthesis the morphologies and facets exposed, wether in nanoscale or microscope[3, 4].

As a perovskite-type material, $BiFeO_3$ was used as the visible-light photocatalyst due to its narrow band gap of 2,2 eV [5, 6]. Especially, the sillenite-type $Bi_{25}FeO_{40}$ with a narrow band gap of 1.8eV exhibit an strong mobility of photogenerated charge, excellent oxidizability of photoinduced holes and enhanced photocatalytic activity, which can be expected as a prospect photocatalysts for the degradation of dyes under visible-light irradia[7, 8]. Hence, many studies have been made in researching synthesis different morphology and size of $Bi_{25}FeO_{40}$ microscope photocatalysts and many remarkable words have been done[9-11]. For example, Feihui Li et al. synthesised magnetically recyclable Bi/$Bi_{25}FeO_{40}$-C nanocomposites by a one step hydrothermal approach. The Bi/$Bi_{25}FeO_{40}$-C showed enhanced photocatalytic activity in hydrogen generation and exhibited high catalytic efficiency, good reusability in p-nitrophenol reduction[12]. Magnetic $Bi_{25}FeO_{40}$-graphene photocatalysts were prepared through a one-step alkaline hydrothermal method and exhibited high catalytic activity for the degradation of methylene blue (MB) under visible-light irradiation[13].

In this work, $Bi_{25}FeO_{40}$ cluster microspeheres catalysts were synthesised using a simple hydrogenthermal method. For comparison, pure $Bi_{25}FeO_{40}$ nanopaticles were prepared by a sol-gel reaction. The catalyst activity of $Bi_{25}FeO_{40}$ photocatalysts were investigated by the photo-Fenton degradation RhB under visible light. The factors influential to the efficiency of photo-Fenton process are also studied and discussed in detail.

II. EXPERIMENTAL

2.1 Synthesis of catalyst.

$Bi_{25}FeO_{40}$ was synthesized via a normal hydrothermal process. In a typical procedure, a certain amount of $Fe(NO_3)_3.9H_2O$ (2,04 g) and $Bi(NO_3)_3.5H_2O$ (2,62 g) were dissolved in 60ml of deionized water under magnetic stirring. The precipitate was put into a Teflon-lined autoclave, followed by adding 10 mL of sodium

alginate solution (10 g/L), 4.5g of citric acid and a certain amount of KOH. After 30 min ultrasonic treatment, the mixture was transferred into a Teflon liner of 100mL capability. The autoclave was sealed and heated at 180 ℃ for 12h and cooled to room temperature naturally. The resulting precipitant was recovered by filtration, followed by washing with distilled water three times, and drying at 80 ℃ for 10h.

2.2 Characterization

X-ray diffraction (XRD analysis was carried out an using X-ray powder diffractometer with Cu Kα radiation at 40 kV and 40 mA. The morphology and internal structure of the prepared samples were further checked by transmission electron microscopy (FESEM), using a JEM 2100F electron microscope operated at a voltage of 200 kV. The element composition of the as-prepared samples was investigated by ICP-MS method. UV–vis reflectance spectra of the powder catalysts were recorded by a Perkin Elmer spectrometer Lambda 35 using an RSAPE-20 reflectance spectroscopy accessory (Labsphere Inc., NorthSutton, NH).

2.3 Heterogeneous photo-Fenton degradation of RhB

The degradation experiments were carried out under single wavelength light (PL-LED 100F λ=410 nm). RhB were used as the model pollutant to evaluate the Fenton activity of the $Bi_{25}FeO_{40}$ sample. In a typical process , 0.1g of $Bi_{25}FeO_{40}$ catalyst was added into 100mL of the RhB (10mg/L) aqueous solution with continuous stirring. Before illumination, the suspension was string in dark for 0.5h to reach adsorption-desorption equilibrium 0.1ml of the H_2O_2 aqueous solution (30%) was added to the reaction solution at the beginning of the illumination. At a defined time interval ,about 5ml of the suspension were collected and centrifuged to remove the catalyst for UV-vis spectrum measurement.

III. RESULT AND DISCUSSION

3.1 XRD analysis

The phase composition and crystallinity of the as-synthesized products were checked by power X-ray diffraction (XRD). As shown in the Fig 1, the diffraction peaks of samples were observed agree with the sillenite-type of $Bi_{25}FeO_{40}$ (JCPDS 46-0416). The strong and sharp diffraction peaks signify exhibit the high crystallinity of $Bi_{25}FeO_{40}$ [14]. It is worth noting that impurity peaks were not found. Compared with the standard pattern, all the diffraction peaks are obviously widened but no preferential orientation is observed in the measured XRD pattern, suggesting the presence of very small hematite crystallites in the products. The average size of the products deduced from Sherrer's formula for the strongest peak (104) is about 25.6 nm. The results suggest that well-crystallized single phase $Bi_{25}FeO_{40}$ has been successfully manufactured.

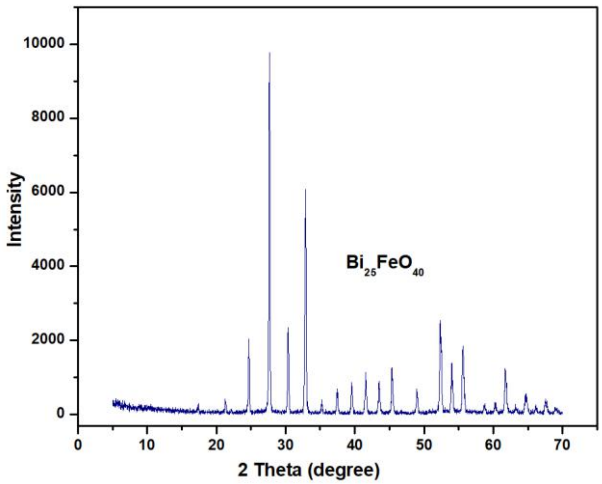

Fig.1. XRD pattern of $Bi_{25}FeO_{40}$ cluster microspheres

3.2 SEM and FESEM analysis

The surface properties of $Bi_{25}FeO_{40}$ photocatalysts were observed using SEM and FESEM methods. The obtained results are depicted in Fig. 2. As shown in Fig. 2a, the material is composed of a large quantity of well-dispersed spherical particles. These particles have uniform size and shape, most of which are spheres of 300-500 nm. In addition, the FESEM image (Fig. 2c) of an individual spherical particle expose that these $Bi_{25}FeO_{40}$ particles are colloidal nanocrystal clusters with a hierarchical architecture, and were built up from many single crystallites of approximately 25 nm in size. The average crystallite size observed from the SEM image, which are consistent with the calculation result from the XRD pattern. In particular, it can be seen products are composed of nanocrystal species through the ordered assembly.

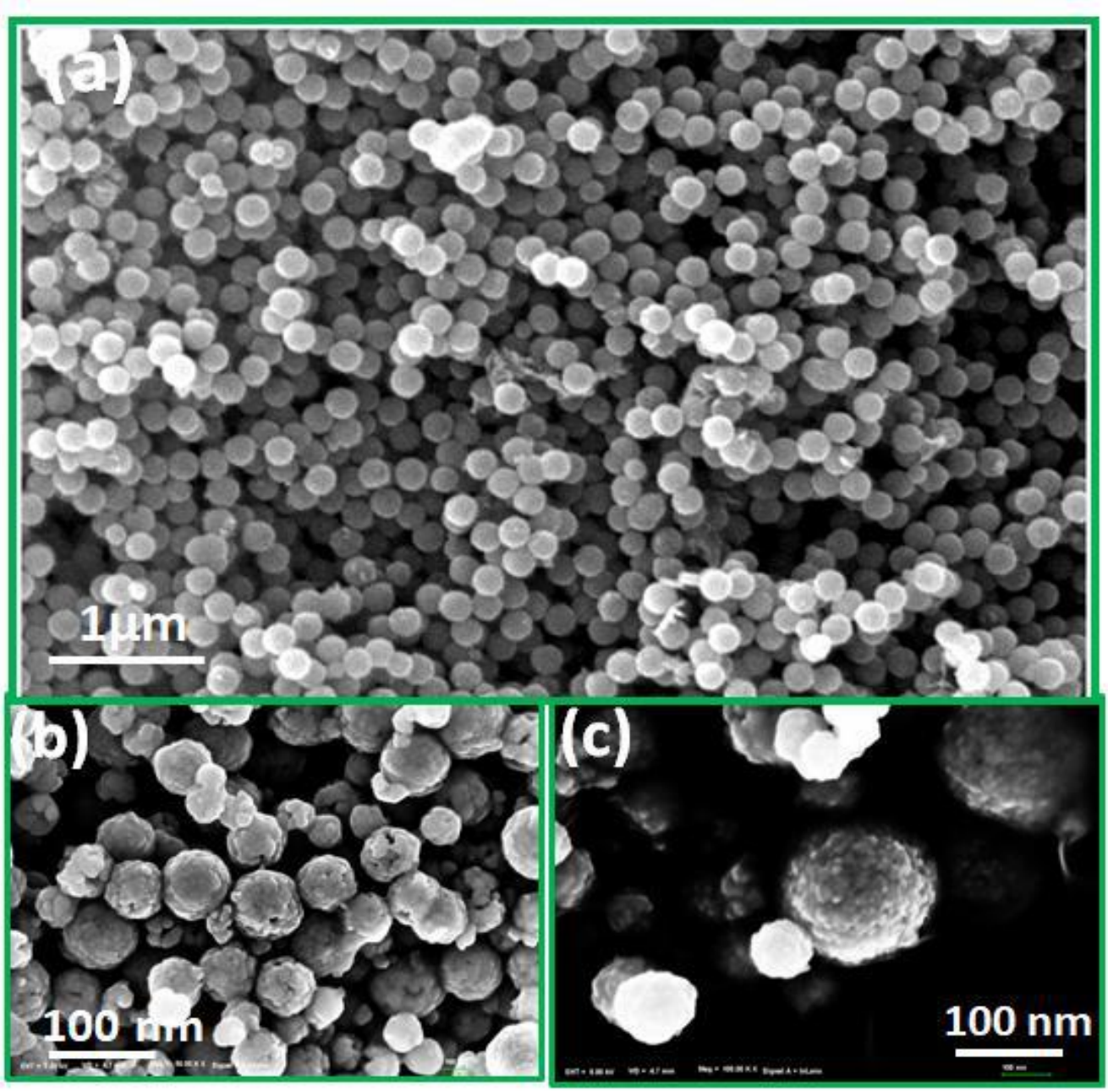

Fig.2. SEM and FESEM image of the as-prepared $Bi_{25}FeO_{40}$ cluster microspheres

3.3 Photo-Fenton degradation of RhB

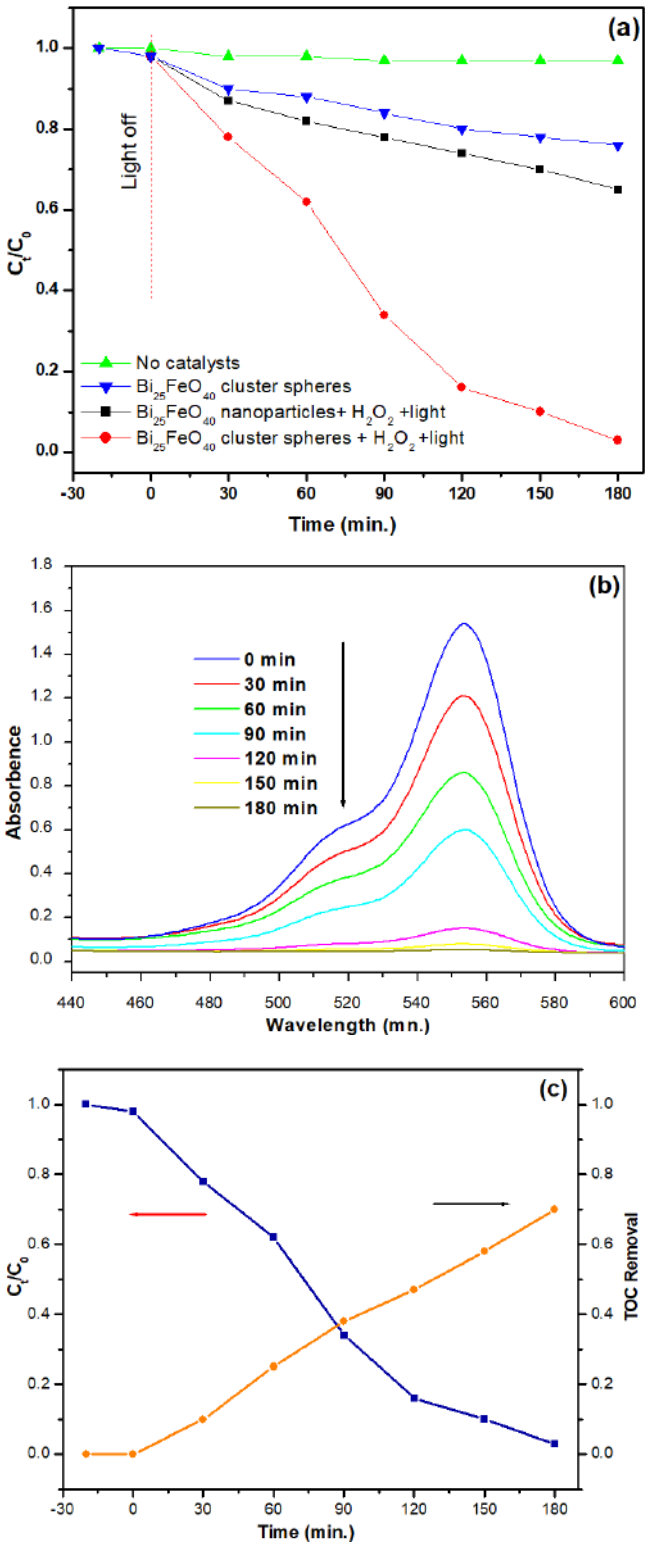

Fig.3. (a) The photocatalytic RhB degradation of the $Bi_{25}FeO_{40}$ catalysts,

The photocatalytic reaction of the $Bi_{25}FeO_{40}$ catalysts were evaluated through the degradation of rhodamine B (RhB) in the presence of H_2O_2 with visible-light. To survey the photocatalytic activity of the as-prepared cluster microspheres, the results are compared with the efficiency of $Bi_{25}FeO_{40}$ nanoparticles. The results of photocatalytic activities of the samples prepared at different conditions are shown in Fig. 3. When the photocatalyst is added but absence of H_2O_2 only slight photodegradation can be observed. The above experiments demonstrate that in this case, the degradation of RhB needed both catalysts and H_2O_2. The photocatalytic activity of the $Bi_{25}FeO_{40}$ photocatalyst with visible light is further investigated by comparison with that of $Bi_{25}FeO_{40}$ nanoparticles[15]. The octahedrons are much more photocatalytically efficient than $Bi_{25}FeO_{40}$ nanoparticles. As shown in Fig.3a, about 96.5 % of RhB is photodegraded for 180 minutes of visible light irradiation while only 36% of RhB reduced with $Bi_{25}FeO_{40}$ nanoparticles and $Bi_{25}FeO_{40}$ cluster microspheres used**,** respectively. The excellent photocatalytic performance of $Bi_{25}FeO_{40}$ cluster microspheres can be attributed to their high crystalline structure and cluster-shaped. Fig. 3b displays the absorption spectra of the RhB solution show a characteristic peak at 550 nm. From Fig 3b, The decreasing intensity of the absorption peak at 550 nm gradually can be observed with time reaction. At a reaction time of 180 minutes the absorption peak intensity is minimal, demonstrating that the RhB was removed. The mineralization of RhB was also investigated as depicted in Fig. 3c. The results reveal that the TOC removal of RhB using $Bi_{25}FeO_{40}$ cluster microspheres as catalysts achieved about 72.5%. The results suggest that as-synthesized cluster microspheres exhibit high capacity for the mineralization of contaminants[16, 17].

Effect of catalyst amount and pH in the range of 2 to 8 on RhB degradation efficiency was also checked (as shown in Figure 4). The results show that the degradation rate of RhB enhanced with an increase in catalyst amount, as depicted in Fig. 4a. However in higher catalyst dosage, the dye removal percentage slightly decreased. Based on the experiment, 2.0 mg of $Bi_{25}FeO_{40}$ cluster microspheresas is optimum dose for the RhB photo-degradation. The experiment results on the effect of pH reveal that the optimum pH was 6.0 (seen at Fig. 4b). With pH below 6.0, in high H^+ concentration, the formation of stable oxonium ion $[H_3O_2]^+$ makes hydrogen peroxide more stable and then decreases its activity with ferrous ions [18]. Moreover, the formation of Fe(II) complexes and ferric oxyhydroxides precipitation at a pH above 5.8 are probably reasons for efficiency decreases in the photo-Fenton RhB removal processes [19].

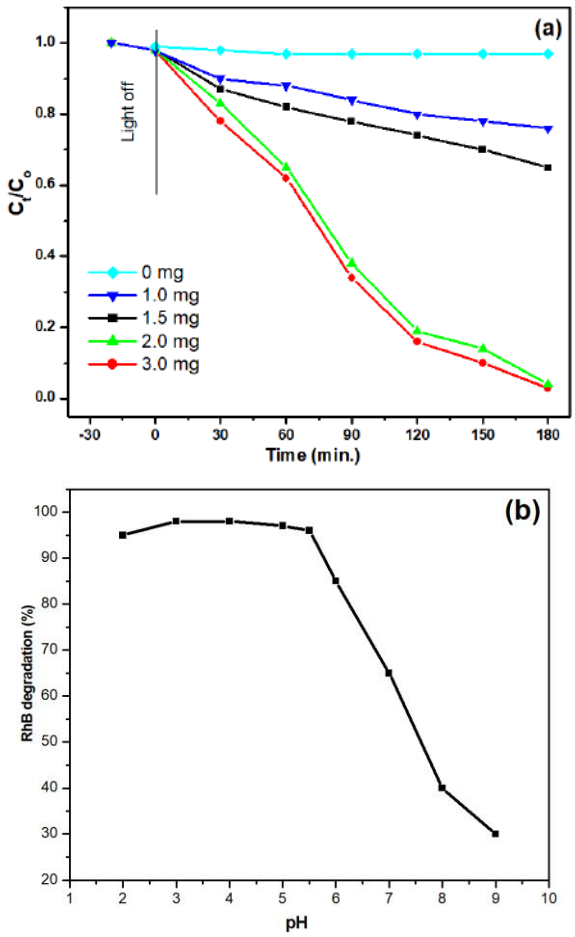

Fig.4. The effect of (a) catalyst amount and (b) pH on RhB removal %

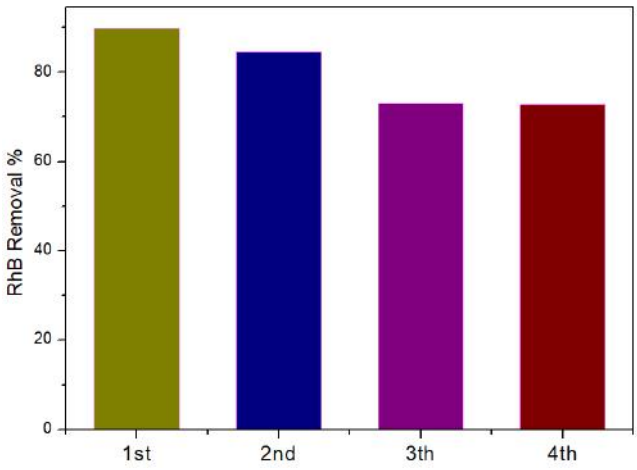

Fig.5. Stability test of the $Bi_{25}FeO_{40}$ sample for photo-Fenton RhB degradation

In addition, the recycle tests were conducted to observe the stability of the as-obtained products in the photo-Fenton degradation RhB process under Vis light irradiation as shown in Fig. 5. The results demonstrate that the used photocatalysts can be collected easily by an internal magnet and the RhB degradation effectively has no significant change during the four successive cycles. The experiments indicate the high stability of the catalyst. These properties play a very important role in application for water treatment at industry scale. The high photocatalytic activity, the stability and the easy separation suggest that the $Bi_{25}FeO_{40}$ cluster spheres can be promising candidates for the photo-Fenton degradation application.

IV. CONCLUSION

$Bi_{25}FeO_{40}$ cluster microspeheres catalysts have been fabricated successfully via a simple one-step hydrogenthermal method. The as-prepare $Bi_{25}FeO_{40}$ particles are colloidal nanocrystal clusters with a hierarchical architecture, and were built up from many single crystallites of approximately 25 nm in size. The $Bi_{25}FeO_{40}$ cluster spheres show the photocatalytic activity higher than that of pure $Bi_{25}FeO_{40}$ nanopaticles by the photo-Fenton degradation RhB under visible light. The results also demonstrate the high stability of the catalyst and the used photocatalysts can be collected easily by an internal magnet.

REFERENCES

[1] Ahsaan Bari MI, Ali Haider, Anwar Ul-Hamid, Junaid Haider, Iram Shahzadi, Ghazanfar Nazir, Anum Shahzadi, M. Imranh, Abdul Ghaffari. (2022). Evaluation of bactericidal potential and catalytic dye degradation of multiple morphology based chitosan/polyvinylpyrrolidone-doped bismuth oxide nanostructures. Nanoscale Adv, 4, 2713-2728.

[2] Garg S, Yadav M, Chandra A, Hernadi K. (2019). A Review on BiOX (X= Cl, Br and I) Nano-/Microstructures for Their Photocatalytic Applications. J Nanosci Nanotechnol, 19, 280-294.

[3] Luo L, Lin H, Li L, Smirnova TI, Maggard PA. (2014). Copper-organic/octamolybdates: structures, bandgap sizes, and photocatalytic activities. Inorg Chem, 53, 3464-3470.

[4] Alam U, Khan A, Bahnemann D, Muneer M. Synthesis of iron and copper cluster-grafted zinc oxide nanorod with enhanced visible-light-induced photocatalytic activity. (2018). J Colloid Interface Sci, 509, 68-72.

[5] Benalioua B, Mansour M, Bentouami A, Boury B, Elandaloussi el H. (2015). The layered double hydroxide route to Bi-Zn co-doped $TiO_{(2)}$ with high photocatalytic activity under visible light. J Hazard Mater, 288, 158-167.

[6] Bhunia MK, Das SK, Dutta A, Sengupta A, Bhaumik A. (2013). Fine dispersion of $BiFeO_3$ nanocrystallites over highly ordered mesoporous silica material and its photocatalytic property. J Nanosci Nanotechnol,13, 2557-2565.

[7] Wen Z W, Bed Poudel, Yi Ma, Z. F. Ren. (2006). Shape Control of Single Crystalline Bismuth Nanostructures. J Phys Chem B, 110, 25702-25706.

[8] Bharathkumar S, Sakar M, K RV, Balakumar S. (2015). Versatility of electrospinning in the fabrication of fibrous mat

and mesh nanostructures of bismuth ferrite ($BiFeO_3$) and their magnetic and photocatalytic activities. Phys Chem Chem Phys, 17, 17745-17754.

[9] Bai Y, Ye L, Chen T, Wang L, Shi X, Zhang X. (2016). Facet-Dependent Photocatalytic N_2 Fixation of Bismuth-Rich Bi_5O_7I Nanosheets. ACS Appl Mater Interfaces, 41, 27661–27668

[10] Arthur R B, Bonin J L, Ardill L P, Rourk E J, Patterson H H, Stemmler E A.(2018). Photocatalytic degradation of ibuprofen over BiOCl nanosheets with identification of intermediates. J Hazard Mater, 358, 1-9.

[11] Zhou D, Yang H, Tu Y, Tian Y, Cai Y, Hu Z, et al. In Situ Fabrication of Bi2Ti2O7/TiO2 Heterostructure Submicron Fibers for Enhanced Photocatalytic Activity. Nanoscale Res Lett. 2016;11:193.

[12] Li F, Zhou J, Gao C, Qiu H, Gong Y, Gao J. (2020). A green method to prepare magnetically recyclable $Bi/Bi_{25}FeO_{40}$-C nanocomposites for photocatalytic hydrogen generation. Appl Surf Sci, 521,146342.

[13] Basith MA, Ahsan R, Zarin I, Jalil MA.(2018). Enhanced photocatalytic dye degradation and hydrogen production ability of $Bi_{25}FeO_{40}$-rGO nanocomposite and mechanism insight. Sci Rep, 8,11090-1198.

[14] Abdullah A H, Moey H J, Yusof N A. (2012). Response surface methodology analysis of the photocatalytic removal of Methylene Blue using bismuth vanadate prepared via polyol route. J Environ Sci, 24, 1694-1701.

[15] Ali I, Han G B, Kim J O. (2018). Reusability and photocatalytic activity of bismuth-TiO_2 nanocomposites for industrial wastewater treatment. Environ Res, 170, 222-229.

[16] Chen S, Huang D, Xu P, Gong X, Xue W, Lei L. (2019). Facet-Engineered Surface and Interface Design of Monoclinic Scheelite Bismuth Vanadate for Enhanced Photocatalytic Performance. ACS Catalysis, 10, 1024-1059.

[17] Ding L, Chen H, Wang Q, Zhou T, Jiang Q, Yuan Y. (2016). Synthesis and photocatalytic activity of porous bismuth oxychloride hexagonal prisms. Chem Commun, 52, 994-997.

[18] Chen C C, Fu J Y, Chang J L, Huang S T, Yeh T W, Hung J T.(2018). Bismuth oxyfluoride/bismuth oxyiodide nanocomposites enhance visible-light-driven photocatalytic activity. J Colloid Interface Sci, 532, 375-386.

[19] Bao Y, Lim T T, Goei R, Zhong Z, Wang R, Hu X. (2018). One-step construction of heterostructured metal-organics@Bi_2O_3 with improved photoinduced charge transfer and enhanced activity in photocatalytic degradation of sulfamethoxazole under solar light irradiation. Chemosphere, 205, 396-403.